

Properties of thick discs formed in clumpy galaxies

Shigeki Inoue^{1,2*} & Takayuki R. Saitoh³

¹*Korea Astronomy and Space Science Institute 776, Daedeokdae-ro, Yuseong-gu, Daejeon, 305-348, Republic of Korea*

²*Racah Institute of Physics, The Hebrew University, Jerusalem, 91904, Israel*

³*Interactive Research Center of Science, Tokyo Institute of Technology, 2-12-1 Ookayama, Meguro, Tokyo 152-8551, Japan*

2013 November 11

ABSTRACT

We examine a possible formation scenario of galactic thick discs with numerical simulations. Thick discs have previously been argued to form in clumpy disc phase in the high-redshift Universe, which host giant clumps of $\lesssim 10^9 M_\odot$ in their highly gas-rich discs. We performed N -body/smoothed particle hydrodynamics simulations using isolated galaxy models for the purpose of verifying whether dynamical and chemical properties of the thick discs formed in such clumpy galaxies are compatible with observations. The results of our simulations seem nearly consistent with observations in dynamical properties such as radial and vertical density profiles, significant rotation velocity lag with height and distributions of orbital eccentricities. In addition, the thick discs in our simulations indicate nearly exponential dependence of σ_θ and σ_z with radius, nearly isothermal kinematics in vertical direction and negligible metallicity gradients in radial and vertical directions. However, our simulations cannot reproduce altitudinal dependence of eccentricities, metallicity relations with eccentricities or rotation velocities, which shows striking discrepancy from recent observations of the Galactic thick disc. From this result, we infer that the clumpy disc scenario for thick-disc formation would not be suitable at least for the Milky Way. Our study, however, cannot reject this scenario for external galaxies if not all galaxies form their thick discs by the same process. In addition, we found that a significant fraction of thick-disc stars forms in giant clumps.

Key words: methods: numerical – galaxies: formation – Galaxy: disc – Galaxy: formation.

1 INTRODUCTION

Duplex structures of thin and thick discs seem to be ubiquitous among disc galaxies (e.g. Burstein 1979; Dalcanton & Bernstein 2002; Yoachim & Dalcanton 2006), including the Milky Way (MW) (e.g. Yoshii 1982; Gilmore & Reid 1983). Because thick-disc stars are generally old and α -enhanced population which implies their early and rapid formation (e.g. Allende Prieto et al. 2006; Haywood et al. 2013), structures of the thick discs are expected to reflect galactic formation history. The origin of the thick discs is, however, still an open question, and a number of possible formation scenarios have been proposed so far. Ones frequently discussed in recent studies are as follows: stellar accretion from disrupted satellites (e.g. Abadi et al. 2003), thickening of a thin disc by minor mergers (e.g. Quinn et al. 1993; Kazantzidis et al. 2008), multiple gas-rich minor mergers (Brook et al. 2004, 2005, 2012), and radial migration by spiral arms and barred structures in a disc (e.g.

Schönrich & Binney 2009a,b). Sales et al. (2009) have discussed that distribution of orbital eccentricities of thick-disc stars reflects their formation processes and can be used as a probe of these scenarios. Afterwards, some observations were performed for the thick disc of the MW and elucidated that the thick-disc stars have a mono-modal distribution with the peak at the eccentricity of $\simeq 0.2$ (Dierickx et al. 2010; Lee et al. 2011; Casetti-Dinescu et al. 2011; Ruchti et al. 2011; Kordopatis et al. 2011, 2013). They argued that the multiple gas-rich minor mergers would be a favourable scenario for the Galactic thick-disc formation, and the radial migration scenario could also reproduce the eccentricity distribution in acceptable matching. On the other hand, the stellar accretion scenario results in relatively higher eccentricities than the observations, and the thin-disc thickening by dwarf galaxies seems to bring about a bi-modal distribution. In addition, observations of Lee et al. (2011) found that correlations between metallicities and some kinematic properties are obviously different between the Galactic thin and thick discs.

* E-mail: shigeki.inoue@mail.huji.ac.il

observed to be clumpy¹, and they have giant clumps the masses of which are $\lesssim 10^9 M_\odot$ in their highly gas-rich discs (e.g. van den Bergh et al. 1996; Elmegreen et al. 2004; Förster Schreiber et al. 2006; Genzel et al. 2006; Guo et al. 2012; Buitrago et al. 2013; Tadaki et al. 2014). Numerical simulations demonstrated the evolution from clump clusters to disk galaxies (e.g. Noguchi 1998, 1999; Immeli et al. 2004; Bournaud et al. 2007; Agertz et al. 2009; Dekel et al. 2009; Ceverino et al. 2010; Mandelker et al. 2013). In the evolutionary process, giant clumps fall into the galactic centre by dynamical friction and can eventually form a galactic bulge (Noguchi 1998, 1999; Elmegreen et al. 2008a; Inoue & Saitoh 2012; Dekel & Krumholz 2013; Bournaud et al. 2014; Perez et al. 2013). In addition, the clumps are so massive that they can change dark matter (DM) density profiles (Elmegreen et al. 2008b; Inoue & Saitoh 2011; see also Del Popolo & Hiotelis 2014) and induce significant net rotation of halo stars and globular clusters around galactic discs (Inoue 2013).

Noguchi (1996) has pointed out the possibility of thick-disc formation in such a clumpy phase of galaxy evolution: Orbital motions of giant clumps kinematically can heat up a galactic disc, and disrupted clumps supply stars to the thick disc to some extent. Afterwards, Bournaud et al. (2009) demonstrated it by numerical simulations. Their numerical simulations showed that the clumpy disc scenario can reproduce observed thick discs with exponential density profiles (see also Bournaud et al. 2007; Elmegreen & Struck 2013) and scale heights independent from radius. Thick discs of external galaxies were indeed observed to have a constant thickness (van der Kruit & Searle 1981; Jensen & Thuan 1982; Shaw & Gilmore 1990; Matthews 2000; Dalcanton & Bernstein 2002). They suggested that the reproducibility of the constant thickness is a characteristic point of this formation scenario; the thin-disc thickening by minor mergers lead to flaring of thick discs in outer disc regions (e.g. Kazantzidis et al. 2008). Observations also seemed to show that the disc-like structures in the clumpy galaxies are consistent with thick discs in nearby galaxies in their thickness and age (Elmegreen & Elmegreen 2005, 2006), and spatial distributions of clumps are nearly exponential although surface brightness profiles of the discs are clearly not (Elmegreen et al. 2005). Thus, it could be said that the thick-disc formation in clumpy galaxies is also a possible scenario and should be examined in detail. However, the properties of the thick discs formed in this scenario have not been compared with observations in the way of Sales et al. (2009).

In this study, we performed several runs of high-resolution N -body/smoothed particle hydrodynamics (SPH) simulation using isolated models and study dynamical and chemical properties of thick discs formed in the clumpy disc scenario. Our aim in this paper is to scrutinize the credibility of this thick-disc formation scenario and discuss whether we can verify or discard the scenario. We describe our simulation settings in §2 and analyses of the thick-disc properties in §3. We present discussion and conclusions in §4 and §5.

¹ These discy galaxies are often called clump clusters, tadpole and chain galaxies according to their inclinations.

2 SIMULATION

The detailed description of our computing schemes has been presented in Inoue & Saitoh (2011, 2012), therefore we describe it briefly here. We employed an N -body/SPH code, **ASURA** (Saitoh et al. 2008, 2009) using the standard scheme of Monaghan (1992) and Springel (2010).² The code adopts the time-step limiter of Saitoh & Makino (2009) so that we can handle strong shocks with an individual time-step method (McMillan 1986; Makino 1991). It also employs the FAST method (Saitoh & Makino 2010) which accelerates the simulations by using different time-steps for the gravitational and hydrodynamical parts. Gravity is solved by a parallel tree with GRAPE (GRAvity PipE) method (Makino 2004; Tanikawa et al. 2013).

A metallicity-dependent cooling function of gas assumes optically thin radiative cooling and covers a temperature range of $10 - 10^8$ K (Wada et al. 2009). Feedback from a uniform far-ultraviolet radiation were taken into account. A gas particle spawns a stellar particle the mass of which is one-third of the initial gas particle under the criteria: 1) $\rho_{\text{gas}} > 100 \text{ atm cm}^{-3}$, 2) temperature $T < 100$ K, 3) $\nabla \cdot \mathbf{v} < 0$ and 4) there are no SNe around the particle. The local star formation rate follows the Schmidt law (Schmidt 1959). We assumed the Salpeter initial mass function (Salpeter 1955) ranging from $0.1 M_\odot$ to $100 M_\odot$ on a stellar particle and that stars heavier than $8 M_\odot$ cause type-II SNe, return their masses to ambient gas and inject thermal energy into it at the rate of 10^{51} erg per SN. The initially primordial gas is contaminated with heavy elements released from the SNe. Our simulation code tracks only the total metal abundance, Z , and does not follow the evolution of each element. We did not take type-Ia (or other) SNe or stellar wind from intermediate mass stars into account in our simulation.

Our initial condition followed the spherical models of Kaufmann et al. (2006, 2007) and Teyssier et al. (2013) that have been used to study the formation of disc galaxies in isolated environments. We assumed equilibrium systems with the Navarro-Frenk-White profile (Navarro et al. 1997, hereafter NFW) with a virial mass of $M_{\text{vir}} = 5.0 \times 10^{11} M_\odot$, a virial radius of $r_{\text{vir}} = 1.67 \times 10^2$ kpc and a concentration parameter of $c = 6.0$. Baryon mass fractions of the systems are set to 0.06. The baryonic components are initially primordial (zero-metal) gas with virial temperature and follows the same density profile as the DM. We executed four runs of simulations with different initial conditions for the gas spheres: two spin parameters of $\lambda = 0.04$ and 0.1, two types of angular momentum distributions (see below). The choice of $\lambda = 0.04$ is motivated by the averaged spin parameter of DM haloes in pure N -body cosmological simulations (e.g. Bullock et al. 2001; Ishiyama et al. 2013). However, observational measurements of spin parameters of high-redshift galaxies are still challenging and debated; for instance, Dutton et al. (2011) advocated consistency with the results of the pure DM simulations, whereas Bouché et al. (2007) proposed $\lambda \simeq 0.1$ on average for star-

² Although the latest version of **ASURA** uses a density-independent SPH scheme (Saitoh & Makino 2013) and a symmetric form of the Plummer softening (Saitoh & Makino 2012), the simulations in this study were performed with the standard SPH and the ordinary softening.

Table 1. Summary of initial conditions of our simulations. From left to right, the columns are simulation names, spin parameters and radial distributions of specific angular momentum. The other parameters are the same in all runs.

run	λ	$j(r)$
B01- λ 004	0.04	$j \propto r$
B01- λ 010	0.1	$j \propto r$
K11- λ 004	0.04	$j \propto r$ in $r < 0.1r_{\text{vir}}$, $j = j(0.1r_{\text{vir}})$ in $r > 0.1r_{\text{vir}}$
K11- λ 010	0.1	$j \propto r$ in $r < 0.1r_{\text{vir}}$, $j = j(0.1r_{\text{vir}})$ in $r > 0.1r_{\text{vir}}$

forming galaxies in the high-redshift Universe (see also Kimm et al. 2011). Hence, we adopt this value as another choice of the initial spin parameters. As for the angular momentum distributions, the pure N -body simulations indicated specific angular momenta of haloes follow the profile of $j \propto r$ in all radial ranges (Bullock et al. 2001). On the other hand, Kimm et al. (2011) performed cosmological simulations including baryonic physics and showed that specific angular momentum distributions of gas follow those of DM inside $0.1r_{\text{vir}}$ and are constant outside $0.1r_{\text{vir}}$; moreover, they found that this distribution is almost independent of redshift. Therefore, we take these two cases as initial conditions of angular momentum distributions. Table 1 summarises our initial settings of the gas spheres.³ Although some of them might be unrealistic, we show that properties of the resultant galaxies are qualitatively consistent in all runs (see §3). The DM and the gas are represented by 10^7 and 5.0×10^6 particles, i.e. the masses of the DM and gas particles are $4.7 \times 10^4 M_\odot$ and $6.0 \times 10^3 M_\odot$. Softening lengths are 10 pc for all particles.⁴

3 RESULTS

Fig. 1 displays snapshots of stellar and gas distributions and star-forming regions in the run of B01- λ 004, where the clumpy phase of the disc can be seen in $t \lesssim 2$ Gyr. Fig. 2 shows stellar density maps of the other runs. In K11- λ 004 and K11- λ 010, the formation of clumps may be involved with ‘ring’ instability caused by the initial setting of the angular momentum distributions (Gingold & Monaghan 1983; Cha & Whitworth 2003). We run our simulations until $t = 6$ Gyr except the run of K11- λ 010. Because this run took ~ 8 Gyr to settle into a stable state, we continued the run until $t = 10$ Gyr; in this sense, K11- λ 010 may not be a realistic initial condition since the clumpy phase is too long in comparison to other numerical simulations (Bournaud et al. 2007, 2014; Bournaud & Elmegreen 2009; Dekel et al. 2009; Ceverino et al. 2010, 2012; Dekel & Krumholz 2013; Perez et al. 2013). In the following subsections, we analyse the final state of the galaxies in our simulations.

³ The simulation of B01- λ 010 is the same as in Inoue & Saitoh (2011, 2012).

⁴ Only in B01- λ 010, we used softening lengths of 8 pc and 2 pc for the DM and gas particles; however, we confirmed that the difference of the softening lengths does not change our results.

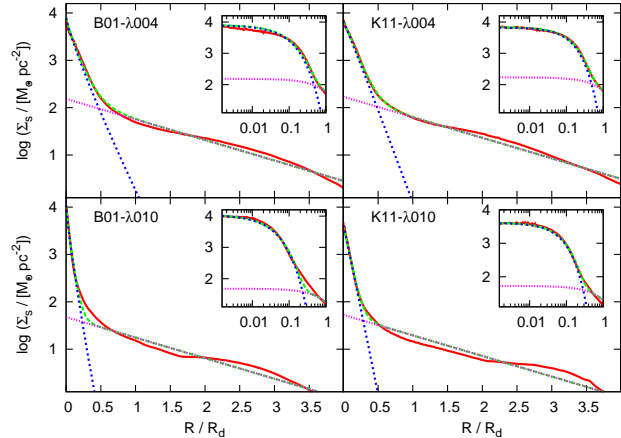


Figure 3. Stellar surface density profiles seen face-on in the final state of our simulations (red lines). Minimum χ^2 fittings are also plotted: Sérsic profiles for bulges (blue short-dashed lines), the exponential profiles for discs (pink dotted lines) and disc+bulge (green long-dashed lines). The insert diagrams illustrate the same profiles with the logarithmic abscissa. The centres of the systems are defined to be the positions at which the stellar densities become the highest.

3.1 Density profiles

3.1.1 Radial profiles

To begin with, we decompose a stellar surface density profile of the simulated galaxy into an exponential disc and a Sérsic bulge,

$$\Sigma_s(R) = \Sigma_d \exp\left(-\frac{R}{R_d}\right) + \Sigma_b \exp\left[-\left(\frac{R}{R_b}\right)^{\frac{1}{n_b}}\right], \quad (1)$$

where $\Sigma_{d,b}$ and $R_{d,b}$ are central surface densities and scale radii of the disc and bulge, and n_b is a Sérsic index of the bulge. The profiles are shown in Fig. 3, and the best-fit parameters and the integrated disc and bulge masses are tabulated in Table 2. The discs of B01- λ 010 and K11- λ 010 have large scale lengths of $\gtrsim 7$ kpc; in this sense, B01- λ 010 and K11- λ 010, i.e. the large spin parameter of $\lambda = 0.1$, may be unsuitable for reproducing MW-like galaxies. Although the disc scale lengths of B01- λ 004 and K11- λ 004 may still be a little larger than that of the MW in recent observations (e.g. Jurić et al. 2008; Bovy et al. 2012c; Bovy & Rix 2013) or within a range of uncertainty (e.g. Cheng et al. 2012a), these are compatible with typical values of disc galaxies (e.g. Kent 1985; Binney & Merrifield 1998; Fathi et al. 2010; Fathi 2010).

In all runs, both the discs and the bulges can be fitted well with exponential profiles: the Sérsic indices of the bulges are $\simeq 1$. Such small Sérsic indices mean that the bulges should be classified into pseudo-bulges (e.g. Kormendy & Kennicutt 2004; Drory & Fisher 2007; Fisher & Drory 2008). However, other studies using numerical simulations with isolated models have supported the formation of classical bulges with high Sérsic indices as remnants of the clump coalescence (Elmegreen et al. 2008a; Perez et al. 2013). In addition, cosmological simulations also seem to indicate $n_b = 3$ –5 (D. Ceverino et al. in prep.). The diversity of the Sérsic indices between these studies and ours may be related to gas fraction of the clumps. If the progen-

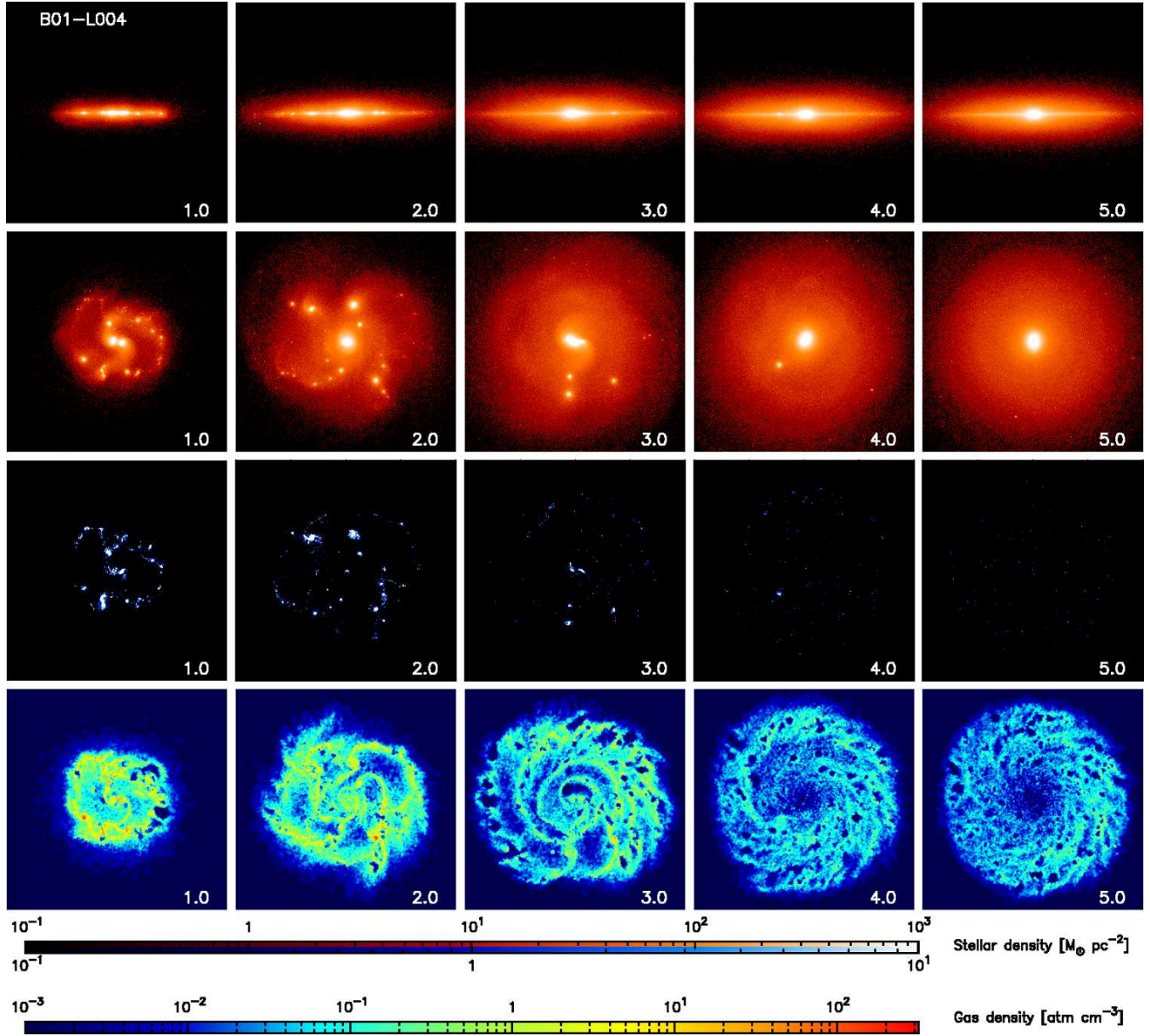


Figure 1. Stellar and gas density maps in the central 40×40 kpc region in the run of B01- λ 004. The first and second rows indicate the surface density of all stars from the edge-on and face-on views, respectively. The third row plots the density of stars younger than 40 Myr as star forming region. The fourth row shows the volume density of gas on the disc plane. Time in units of Gyr is indicated on right bottom corner of each panel.

Table 2. The best-fit parameters for the radial profiles. Surface density profiles of discs and bulges are fitted with equation (1), and M_d and M_b are disc and bulge masses computed by integrating the fitting profiles. f_{gas} is a mass fraction of gas particles to the total baryon in the region of $R < 5R_d$ and $|z| < 5h_T$ in the final state (see equation (2) and Table 3 for h_T).

run	Σ_d [$M_\odot \text{ pc}^{-2}$]	R_d [kpc]	Σ_b [$M_\odot \text{ pc}^{-2}$]	R_b [kpc]	n_b	M_d [M_\odot]	M_b [M_\odot]	f_{gas}
B01- λ 004	1.5×10^2	4.4	7.8×10^3	0.38	1.16	1.9×10^{10}	9.6×10^9	0.07
B01- λ 010	4.8×10	8.1	1.1×10^4	0.24	1.19	2.0×10^{10}	5.8×10^9	0.16
K11- λ 004	1.7×10^2	4.1	6.7×10^3	0.50	0.97	1.8×10^{10}	9.9×10^9	0.04
K11- λ 010	5.3×10	6.8	4.1×10^3	0.44	0.98	1.6×10^{10}	4.7×10^9	0.29

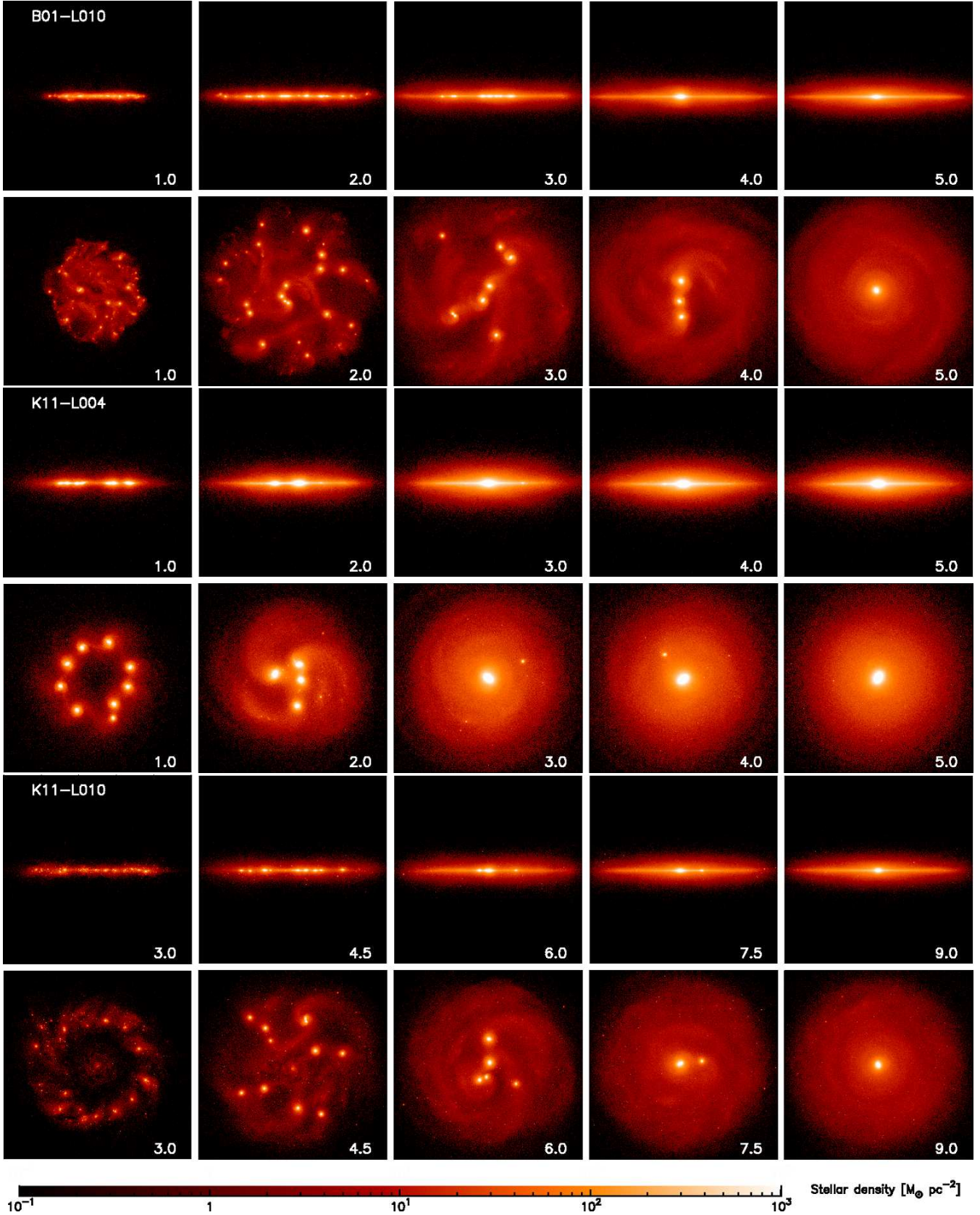


Figure 2. Stellar density maps seen edge-on and face-on in the runs of B01- λ 010, K11- λ 004 and K11- λ 010 from top to bottom. The depicted regions are the central 40×40 kpc region for K11- λ 004 (the third and fourth rows) and 60×60 kpc regions for B01- λ 010 (the first and second rows) and K11- λ 010 (the fifth and sixth rows).

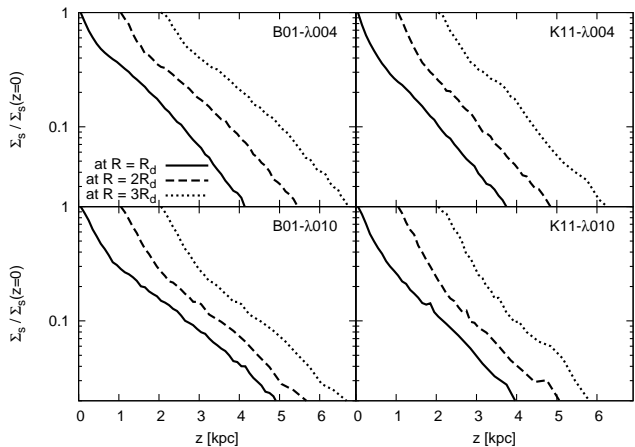


Figure 4. Vertical density profiles of stars in projected edge-on view at the final state of the simulations. The profiles are normalized by the surface density at $z = 0$ and shifted right at intervals of 1 kpc for visibility.

itor clumps and the remnant bulges are gas-rich, the dissipative gas can contract to the centre and may form highly concentrated density profiles, which leads to a high Sérsic index. On the other hand, an opposite expectation may also be possible. High Sérsic indices can be considered as results of violent relaxation of dissipationless mergers like elliptical galaxies. In this case, coalescence of gas-poor clumps may lead to a high Sérsic index, rather than gas-rich clumps. Thus, the dynamical properties of ‘clump-origin bulges’ are to be investigated further in future studies.⁵

3.1.2 Vertical profiles

Fig. 4 shows vertical density profiles of the projected stellar discs at different galactocentric radii. The profiles can be fitted with superposition of two exponential profiles with breaks at $z \simeq 1$ kpc: thin and thick discs. In agreement with the results of Bournaud et al. (2009), vertical scale heights of the thick discs are almost independent from radius in all of our simulations; we found that the variation of the scale heights were smaller than 20 per cent in the range of $1 \leq R/R_d \leq 3$. In addition, scale radii and central densities of the thin and thick discs can be measured by the fitting of the vertical profiles with double-exponential models,

$$\rho_d(R, z) = \sum_i \rho_{0,i} \exp\left(-\frac{R}{R_i} - \frac{|z|}{h_i}\right), \quad (2)$$

where the subscript i takes thin and thick discs, and R_i and h_i are scale radii and scale heights of the discs. The fitting is performed in the range of $1 \leq R/R_d \leq 3$ to avoid the bulge contribution. We found that the scale radii are hardly different between the thin and thick discs. The best-fit parameters and masses of the thin and thick discs are tabulated in Table 3.

In all runs, however, the thick discs are more massive than the thin discs; we found mass ratios of the thick to

⁵ Detailed analysis of the bulge in B01-λ010 has been reported in Inoue & Saitoh (2012).

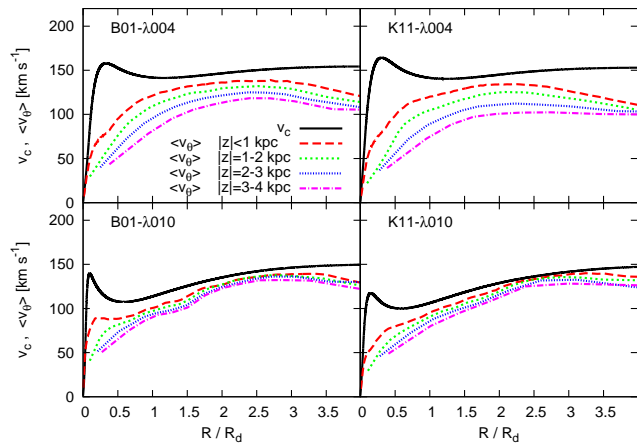


Figure 5. Radial profiles of circular and mean rotation velocities of stars. The circular velocity is computed as $v_c = \sqrt{GM(<R)/R}$, where G is the gravitational constant and $M(<R)$ is the mass of the system spherically enclosed in radius of R . The mean rotation velocity v_{θ} is measured at each height above the plane.

the thin discs to be greater than 2 in all runs. Thick discs have been observed to account for 5–40 per cent of the total stellar masses in real galaxies (Yoachim & Dalcanton 2006). Although Fuhrmann (2008) and Comerón et al. (2011) suggested that typically thick and thin discs have similar masses, the thin discs in our simulations would be still too less massive. This is because our initial conditions assumed single collapse models, do not include late accretion to feed gas to the thin discs after the clumpy disc formation (Bournaud et al. 2009). We warn the reader that this point is a limitation of our simulations. The scale heights of the thick and thin discs are tabulated in Table 3; however, it should be noted that the thick-disc scale heights would be somewhat shortened by the thin-disc formation that is lacked in our simulations (Bournaud et al. 2009). Moreover, the scale radii of the thin discs may become shorter or longer than those of their thick discs after the completion of the thin-disc formation.

3.2 Kinematics

3.2.1 Rotation velocities

Fig. 5 shows radial profiles of circular and mean rotation velocities of stars. The galaxies have nearly flat rotation curves in the runs of B01-λ004 and K11-λ004 in their disc regions, whereas the circular velocities gently increase in B01-λ010 and K11-λ010 (see also Fig. 8). It should be noted, however, that the massive bulges cause the mass concentrations of the galaxies to be high as seen in Fig. 3, and contribution of the bulges to the circular velocity curves would be substantially present in all simulated runs.

The mean rotation velocities in the figure show significant asymmetric drift in the cases of B01-λ004 and K11-λ004: velocity lags of $d\langle v_{\theta} \rangle/dz \sim -10 \text{ km s}^{-1} \text{ kpc}^{-1}$. In B01-λ010 and K11-λ010, however, the velocity lags are weak. In the MW, rotation velocity has been observed to decrease significantly with distance from the plane although determinations do not seem to be consistent quantitatively: from -36 to

Table 3. The best-fit parameters for vertical density profiles with equation (2). Subscriptions of ‘T’ and ‘t’ mean values for thick and thin discs.

run	$\rho_{0,T}$ [$M_\odot \text{ pc}^{-3}$]	R_T [kpc]	h_T [kpc]	$M_{d,T}$ [M_\odot]	$\rho_{0,t}$ [$M_\odot \text{ pc}^{-3}$]	R_t [kpc]	h_t [kpc]	$M_{d,t}$ [M_\odot]	$\frac{M_{d,T}}{M_{d,t}}$
B01- λ 004	3.5×10^{-2}	5.5	1.4	2.0×10^{10}	2.7×10^{-2}	5.5	0.19	2.0×10^9	10.0
B01- λ 010	6.5×10^{-3}	9.8	1.9	1.5×10^{10}	1.4×10^{-2}	9.8	0.45	7.4×10^9	2.1
K11- λ 004	7.3×10^{-2}	4.2	1.1	1.8×10^{10}	6.5×10^{-2}	4.2	0.17	2.5×10^9	7.2
K11- λ 010	1.0×10^{-2}	8.2	1.3	1.1×10^{10}	1.3×10^{-2}	8.2	0.31	3.5×10^9	3.2

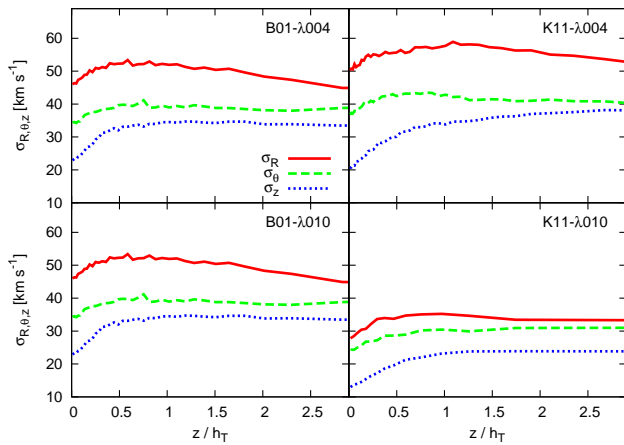


Figure 6. Dispersions of radial, rotation and vertical velocities as functions of distance from the plane at the galactocentric radius of $R = 2R_d$.

$-9 \text{ km s}^{-1} \text{ kpc}^{-1}$ (Chiba & Beers 2000; Carollo et al. 2010; Spagna et al. 2010; Lee et al. 2011; Casetti-Dinescu et al. 2011; Moni Bidin et al. 2012); in this sense, B01- λ 004 and K11- λ 004 seem to be more similar to the MW. Meanwhile, in external galaxies, Yoachim & Dalcanton (2008) have observed that massive galaxies in their sample indicate little differences of rotation velocities between thin and thick discs.

3.2.2 Velocity dispersions

Fig. 6 shows vertical profiles of velocity dispersions. As seen from the figure, the velocity dispersions are almost constant, and the discs can be considered to be isothermal along the vertical direction. Hereafter, we follow the analytical discussion of Lewis & Freeman (1989). If the surface mass density is dominated by the stellar disc and the vertical density profile can be assumed to be a single exponential function, from the Jeans equation with the isothermality,

$$\sigma_z^2(R) \propto \Sigma_s \propto \exp\left(-\frac{R}{R_d}\right) \quad (3)$$

Furthermore, if we assume uniform velocity anisotropy throughout the discs: $\sigma_\theta/\sigma_z \simeq \text{const}$, $\sigma_\theta^2(R) \propto \exp(-R/R_d)$. Finally, if σ_R^2 is exponential with a scale length of R_R ,

$$\frac{\sigma_\theta^2}{\sigma_R^2} = \frac{\sigma_\theta^2(0)}{\sigma_R^2(0)} \exp\left[-R\left(\frac{1}{R_d} - \frac{1}{R_R}\right)\right] = \frac{1}{2} \left(1 + \frac{R}{v_c} \frac{dv_c}{dR}\right), \quad (4)$$

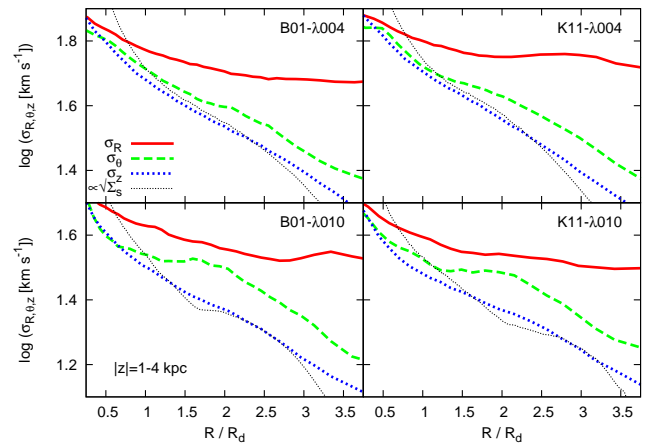


Figure 7. Radial, rotation and vertical velocity dispersions as functions of galactocentric distance. Stars in $1 \text{ kpc} < |z| < 4 \text{ kpc}$ are taken into account for the measurements. For the sake of comparison, normalized profiles of the square roots of stellar surface densities are also plotted with the black thin dotted lines.

where the second equality is derived from the epicyclic approximation (e.g. Binney & Tremaine 2008). In the case of a flat rotation curve, since the right-hand side (RHS) is constant, the two scale lengths must be $R_R = R_d$; moreover, $\sigma_\theta^2/\sigma_R^2 = 1/2$. To summarise, if all of these assumptions hold, it can be expected that

$$\Sigma_s \propto \sigma_R^2 \propto \sigma_\theta^2 \propto \sigma_z^2 \propto \exp\left(-\frac{R}{R_d}\right). \quad (5)$$

To compare our simulations with the above analyses, Fig. 7 shows radial profiles of velocity dispersions of thick-disc stars in our simulations. We confirmed that the profiles hardly depend on height above the plane because of the isothermality shown in Fig. 6. As discussed above, the profiles of σ_θ , σ_z and $\sqrt{\Sigma_s}$ seem to indicate exponential behaviour with nearly similar scale lengths although σ_θ have shallower slopes in $1 < R/R_d < 2$ in B01- λ 010 and K11- λ 010. The decrease of σ_R with radius, however, are much slower than the other profiles and not exponential. This means that the assumption of uniform velocity anisotropy between σ_R and the other dispersions is not valid in the simulated discs. Fig. 8 shows the left- and RHS of equation (4). The ratios of $\sigma_\theta^2/\sigma_R^2$ are not constant and decrease with radius in outer regions although the RHS is $\simeq 1/2$, indicating that the circular velocity curves can be considered to be almost flat. It is particularly worth noting that $\sigma_\theta^2/\sigma_R^2$ largely decrease and deviate from the RHS in $R \gtrsim 2.5R_d$

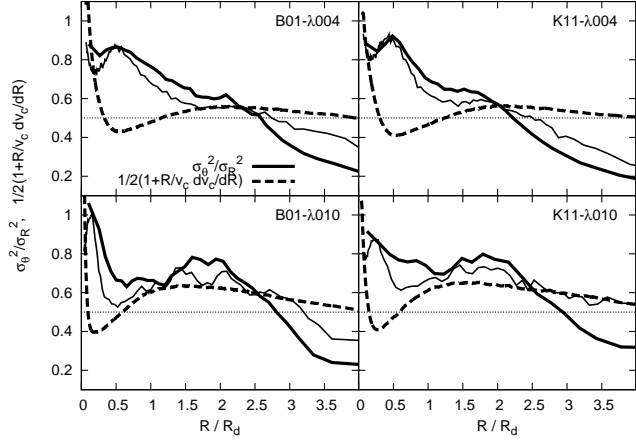


Figure 8. The left- and right-hand sides of equation (4) as functions of radius. The thin and thick lines indicate $\sigma_\theta^2/\sigma_R^2$ for stars in the regions of $|z| < 1$ kpc and $1 \text{ kpc} < |z| < 4$ kpc, respectively. The horizontal dotted-lines indicate $1/2$.

except the region of $|z| < 1$ kpc in K11- λ 010. This implies that the epicyclic approximation would not be valid in the outer disc regions in our simulations. Another notable point in Fig. 7 is that the behaviour of the velocity dispersions are almost the same among the simulation runs.

3.2.3 Distributions of orbital eccentricities

As we mentioned in §1, Sales et al. (2009) have found that distribution of orbital eccentricities of thick-disc stars reflects their formation process. Therefore, it is worthwhile to inquire into eccentricity distributions in our simulations. Following the manner of Sales et al. (2009), we fitted the circular velocity curves of Fig. 5 with combined models of an NFW halo, a Hernquist bulge (Hernquist 1990) and a Miyamoto-Nagai disc (Miyamoto & Nagai 1975). Orbit calculations are executed in the modeled potentials, and peri- and apo-centre distances $r_{\text{pe,ap}}$ are computed, in which the final states of our simulations are used as the initial positions and velocities of the orbit calculations. The orbital eccentricity is defined as $e \equiv (r_{\text{ap}} - r_{\text{pe}}) / (r_{\text{ap}} + r_{\text{pe}})$.

The top panel of Fig. 9 shows the eccentricity distributions in thick-disc regions of $1 \text{ kpc} < |z| < 4$ kpc. These distributions are almost consistent with the observations of the Galactic thick disc. The distributions do not indicate significant dependence on the initial conditions although the peak values are high in B01- λ 010 and K11- λ 010 and the position of the peak tends to be a little high eccentricity in K11- λ 004. The bottom panel of Fig. 9 shows dependence of the distributions on distance from the planes. Although the lowest regions of $|z| < 1$ kpc may have slightly low eccentricities (see below), the thick-disc stars in our simulations do not indicate altitudinal gradients of orbital eccentricities. It is noteworthy that this would be discrepant from observations: Dierickx et al. (2010) observed that mean eccentricities decrease with height in the Galactic thick disc, and their observed distributions become broader in higher regions. We discuss the dependence of this result on the galaxy models in Appendix A and find that the eccentricity distributions

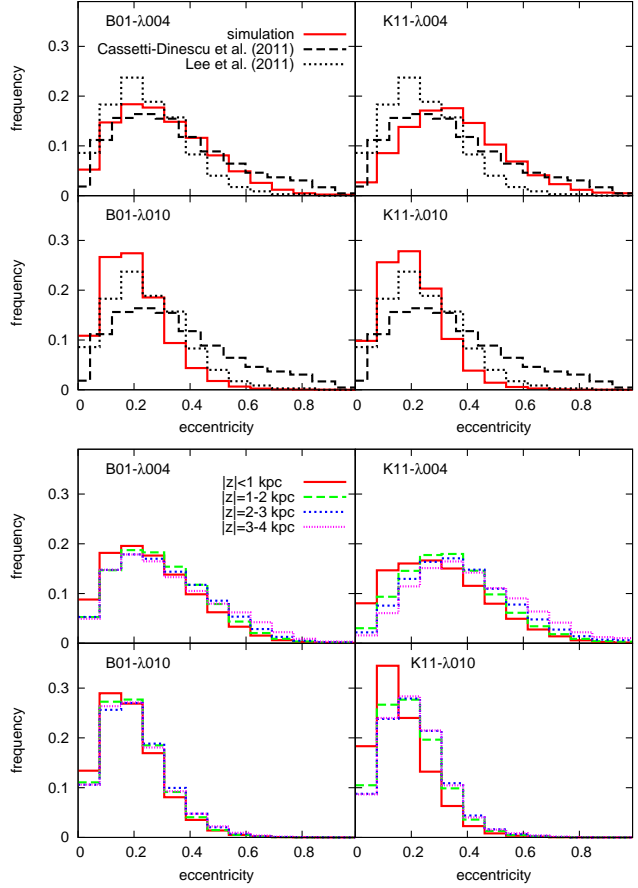


Figure 9. Top: Eccentricity distributions of stars in the region of $2 < R/R_d < 3$ and $1 \text{ kpc} < |z| < 4$ kpc in the final states. Observational results by Lee et al. (2011, in $0.8 \text{ kpc} < |z| < 2.4$ kpc) and Casetti-Dinescu et al. (2011, in $1 \text{ kpc} < |z| < 3$ kpc) are overplotted for comparison. Bottom: Eccentricity distributions at different heights in our simulations.

are qualitatively independent from the details of the galaxy models.

From integration of the fitting profiles of vertical density distributions, thin disc stars occupy stellar mass fractions of 0.17, 0.52, 0.19 and 0.36 in B01- λ 004, B01- λ 010, K11- λ 004 and K11- λ 010 in the lowest regions of $|z| < 1$ kpc. The slightly lower eccentricities in this regions may be due to the contamination of the thin-disc stars if thin-disc stars have more regular kinematics than thick-disc stars.

3.3 Metallicity relations

Metallicity distribution can also be a key to investigate the formation history of the thick-disc stars. Fig. 10 shows radial and vertical distributions of averaged metallicity in our simulations.⁶ In all runs, stars in the thick-disc regions have metallicities similar to the solar value and are more metal-rich than the observed thick-disc stars (e.g. van der Kruit & Freeman 2011, and reference therein). This

⁶ All averaged values are mass-weighted throughout this paper, which are hardly different from the simple mean values of stellar particles.

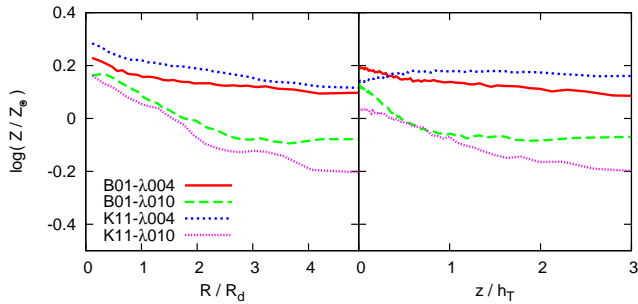


Figure 10. Radial and vertical distributions of mean metallicities of stars. The radial (the right panel) and vertical profiles (the left panel) are measured in $1 \text{ kpc} < |z| < 4 \text{ kpc}$ and $2 < R/R_d < 3$, respectively. We set the solar metallicity to $Z_\odot = 0.02$.

can be attributed to metal-enrichment caused inside the giant clumps since a significant fraction of thick-disc stars are born in massive clumps in our simulations (see §3.4). Thus, the existence of giant clumps during the disc-formation epoch can lead to significantly high metallicity of thick-disc stars; however, it should be noted that the metal-enrichment would depend on the intensity of feedback in the simulations since gas outflow from the clumps could refresh the gas inside them (see §4.1). Besides, the metallicity gradients in our simulations are weak in both radial and vertical directions. This would be because perturbations of massive clumps vehemently stir the disc stars and wash out their metallicity gradients which could have appeared in quiet disc formation. Although the runs of B01-λ010 and K11-λ010 show metallicity gradients in $R \lesssim 2R_d$, the radial variations in metallicities are as small as ~ 0.3 dex. Thus, we expect that the clumpy disc formation would lead to the chemical uniformity of a thick disc if our single collapse models well represent the formation of clumpy galaxies in the high-redshift Universe. The MW thick disc has been observed to have only weak radial and vertical gradients: e.g. $\partial Z/\partial R \simeq -0.003 \pm 0.005 \text{ dex kpc}^{-1}$ (Hayden et al. 2013), and $\partial Z/\partial z \simeq -0.1 \pm 0.05 \text{ dex kpc}^{-1}$ (Kordopatis et al. 2011, 2013) and $-0.26 \pm 0.02 \text{ dex kpc}^{-1}$ (Hayden et al. 2013). Radial and vertical gradients of $[\text{Fe}/\text{H}]$ are observed to be between 0.0028 and $0.041 \text{ dex kpc}^{-1}$ (Nordström et al. 2004; Ruchti et al. 2011; Coşkunoğlu et al. 2012; Cheng et al. 2012b; Carrell et al. 2012) and between -0.14 and $-0.068 \text{ dex kpc}^{-1}$ (Chen et al. 2011; Kordopatis et al. 2011; Katz et al. 2011; Ruchti et al. 2011; Carrell et al. 2012), respectively.

Lee et al. (2011) and Kordopatis et al. (2011, 2013) have recently revealed that orbital eccentricity and rotation velocity seem to correlate with metallicity: ϵ decreases and $\overline{v_\theta}$ increases with metallicity for Galactic thick-disc stars. They found that these chemo-dynamical relations of the thick disc are distinct from those of the thin disc and can be used as proof of thick-disc formation scenarios. Fig. 11 shows these chemo-dynamical relations of thick-disc stars in our simulations. As clearly seen from the figure, neither ϵ nor $\overline{v_\theta}$ indicate correlation with metallicities. In connection to the above discussion, this result can be taken as a natural consequence of the weak gradients of metallicity and eccentricity shown in Fig. 10 and the bottom panel of Fig. 9. Accordingly, we can see that the clumpy disc scenario for

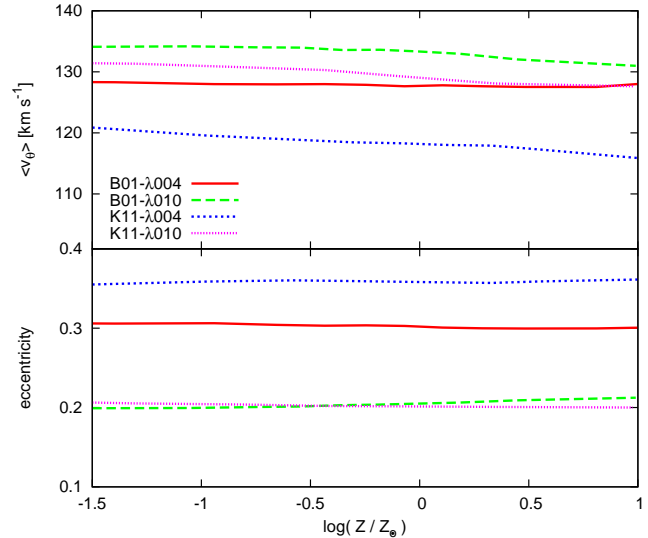


Figure 11. Orbital eccentricities and rotation velocities as functions of metallicities of stars in the region of $2 < R/R_d < 3$ and $1 \text{ kpc} < |z| < 4 \text{ kpc}$.

thick-disc formation could not reproduce the correlations of ϵ and v_θ with metallicity observed in the Galactic thick disc since the violent mixing by massive clumps can erase the metallicity relations.

3.4 Where do thick-disc stars form?

It would be of great worth to discuss how and where the thick-disc stars formed in our simulations. In Fig. 1, intense star formation can be seen in the clumps, and the inter-clump regions scarcely form stars. Notwithstanding, the galactic disc accounts for the greater fraction of the stellar mass in the final state. This implies that the giant clumps supply significant amount of stars to the disc. Giant clumps are totally or partly disrupted by tidal force while migrating toward the galactic centre. Besides, in merging with one another, the clumps scatter the inter-clump regions with stars. Elmegreen et al. (2009) have inferred that some fraction of the clump mass disperses into the inter-clump medium from their observations, and Bournaud et al. (2007, hereafter BEE07) estimated that ~ 20 per cent of disc mass is supplied from massive clumps in their simulations.

Taking advantage of the high mass-resolutions of our simulations, here we compute the mass fractions of stars released from clumps to discs. First, we identify stellar clumps in snapshots every 4 Myr using the friends-of-friends (FOF) method, in which the linking lengths are set to $(m_s/\rho_t)^{1/3}$, where m_s is the mean mass of stellar particles and ρ_t is the stellar density at the radius where surface densities of a bulge and a disc become equal in the fittings of Fig. 3. We found that the results do not depend very much on the linking length within a factor of approximately two. The minimum group (clump) mass m_{min} have to be given in the FOF algorithm, and we treat it as a parameter of the analyses. Here, we define FOF-grouped stars in the final snapshot to be bulge stars and the others to be disc stars. Next, we search for new stars born in the FOF clumps in each snapshot. If the new stars in the clumps are identified to be disc stars in

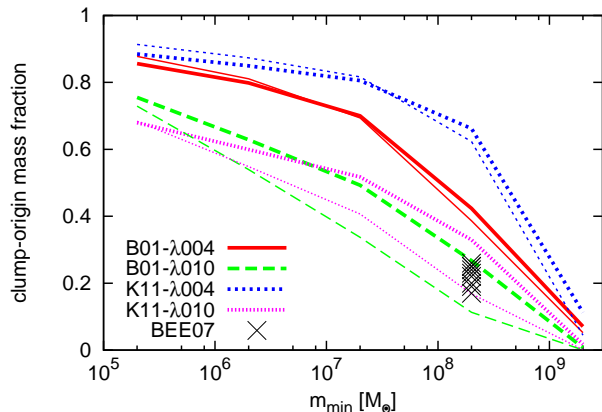


Figure 12. Mass fractions between stars released from clumps to the disc and the final stellar disc. The horizontal axis means minimum clump mass defined in the FOF method. The thick lines are for all disc stars, and the thin lines are for stars in the region of $2 < R/R_d < 3$ and $1 \text{ kpc} < |z| < 4 \text{ kpc}$ in the final snapshot. The \times -marks designate the results of BEE07; however, be aware of their different analysing technique (see the text).

the final snapshot, we consider these stars as the mass supply from the clumps to the disc.⁷ Finally, we sum up the mass supply in all snapshots, estimate the mass ratio between the stars released from the clumps and the final disc at a given m_{min} . The lowest-mass clump of $m_{\text{min}} = 2 \times 10^5 M_{\odot}$ consists of more than one hundred particles.

Fig. 12 shows the results of the analysis as function of m_{min} . We notify readers that this figure indicates mass-contribution cumulated from large to small clumps: steepness of the slopes at a certain m_{min} corresponds to contribution from the clumps having the mass. In the runs of B01- λ 004 and K11- λ 004, massive clumps of $\gtrsim 10^8 M_{\odot}$ largely contribute to disc formation, and the thick discs have almost the same composition as the entire discs. In B01- λ 010 and K11- λ 010, the contribution from smaller clumps is relatively larger than in the other runs, and all mass ranges contribute nearly equally, i.e. relatively straight profiles in the figure. We consider that this variance between the runs could be attributed to the difference of mass functions of clumps (see §4.1). In any runs, it can be said that significant fractions of the thick-discs stars are born in the clumps, and disrupted clumps seem to be a major supplier of stars to galactic discs in our simulations. For comparison, we also show the results of simulations of BEE07 in the figure. Here we have to note that BEE07 have used different clump detection and analysis methods for the sake of fair comparison with observations: They deteriorated resolutions of their face-on density maps down to 200 pc and searched for pixels with high contrast. BEE07 defined regions less extended than 3 kpc and more massive than $2 \times 10^8 M_{\odot}$ as their clumps. Therefore, it should be kept in mind that fairness is not ensured in the comparison between our and BEE07 simulations in Fig. 12.

⁷ Stellar mass loss due to SNe until the end of simulations is taken into account, i.e. the clump identification is performed in each snapshot, but the resultant mass fractions in Fig 12 are computed with masses of stellar particles in the final snapshot.

Our results of B01- λ 010 and K11- λ 010 are nearly consistent with BEE07, but the runs of B01- λ 004 and K11- λ 004 indicate much larger mass contributions from massive clumps of $> 2 \times 10^8 M_{\odot}$.

Fractional mass contribution from clumps of 10^7 – $10^9 M_{\odot}$ thus seems to depend on the initial conditions of our simulations, therefore we could not assert that our simulations represent well the clumpy galaxies in the high-redshift Universe. In addition, feedback processes such as SNe and radiation pressure may be influential on the picture of disc formation and mass function of clumps (Genel et al. 2012; Perez et al. 2013). It is noteworthy, however, that the dynamical and chemical properties shown in the previous subsections were well consistent between the runs although Fig. 12 showed the somewhat diverse results.

4 DISCUSSION

4.1 The validity and robustness of our simulations

First, we have to mention that numerical simulations for star-forming galaxies are still to be developed. Especially, implementation of feedback processes at the sub-grid level have long been debated (e.g. Stinson et al. 2006, 2012; Dalla Vecchia & Schaye 2012; Agertz et al. 2013). Such feedback processes may be crucial for fate of giant clumps. Noguchi (1996) has firstly pointed out the possibility that giant clumps may be transient objects if they are largely losing their mass by outflow. Recently, Genzel et al. (2011) and Newman et al. (2012) observed that some clumps indeed seem to be subjected to such strong outflow. Afterwards, Genel et al. (2012) performed numerical simulations using a parametrised method for representing the superwinds and seemed to show that the clumps could not grow massive and would be disrupted in timescales shorter than their orbital periods. Some other observations also determined young ages of clumps in agreement with the ephemerality of clumps under the strong feedback (e.g. Wuyts et al. 2012; Swinbank et al. 2012). On the other hand, recent analytical studies and numerical simulations have taken the stellar feedback into account, and they seemed to show that giant clumps can accrete ambient gas to keep their masses even under the strong outflow (Krumholz & Dekel 2010; Forbes et al. 2013; Dekel & Krumholz 2013; Bournaud et al. 2014; although see Hopkins et al. 2012). In this case, the clumps are expected to be long-lived and migrate toward the galactic centres. In addition, radial gradients of ages, specific star-formation rates and gas fractions of clumps were observed and could be taken as indicative of the longevity and the migration of clumps (Förster Schreiber et al. 2011; Guo et al. 2012; Tadaki et al. 2014); additionally, Mandelker et al. (2013) confirmed the presence of these radial gradients in their simulations where their clumps are long-lived and form central bulges.

Because the stellar feedback processes have not been implemented in our simulation code yet, star formation rate would possibly be overestimated in the clumpy phase (e.g. Saitoh & Makino 2010; Dalla Vecchia & Schaye 2012; Agertz et al. 2013). The reader should be aware that our results may be sensitive to this issue. Perez et al. (2013)

have performed N -body/SPH simulations using isolated disc models and shown how a mass function of clumps varies with strength of SN feedback between 0 and 1.0×10^{51} erg per SN. They found that a typical clump mass becomes more massive in a run with stronger SN, and the most frequent clump mass in the run with the strongest SN is ~ 0.5 dex larger than in the case excluding the feedback. Thus, less massive clumps are disrupted due to the feedback, whereas massive ones can survive if they grow rapidly. Bournaud et al. (2014) also performed simulations with isolated galaxy models in which they took into account various feedback processes such as HII region photo-ionization, radiation pressure from young stars and non-thermal feedback from SNe. They demonstrated that clumps more massive than $\simeq 10^8 M_\odot$ can survive and keep their masses nearly constant even under the feedback stronger than in our study and Perez et al. (2013); moreover, this result was confirmed in cosmological simulations (N. Mandelker et al. in prep.) In our study, Fig. 12 indicates that more than 50 per cent of the thick-disc stars form in clumps more massive than $10^8 M_\odot$ in the runs of B01- $\lambda 004$ and K11- $\lambda 004$ although the fractions are $\simeq 20$ per cent in B01- $\lambda 010$ and K11- $\lambda 010$. Therefore, it could be expected that the thick-disc properties in B01- $\lambda 004$ and K11- $\lambda 004$ would be robust with respect to the feedback efficiency in simulations. On the other hand, the thick discs in B01- $\lambda 010$ and K11- $\lambda 010$ may not be formed from dissolved clumps if the other feedback processes are implemented. Moreover, bulge masses could also be affected by the feedback. If the feedback dissolves the majority of clumps, the bulges could not grow massive. In this sense, contribution by the bulges to potentials of entire galaxies may depend on the strength of the feedback, thereby the feedback efficiency may be influential on dynamical properties of disc stars via the bulge potentials.

Significance of the metallicity gradients would be affected by the strength of feedback. Cosmological simulations of Gibson et al. (2013) have demonstrated that strong stellar feedback can wash out metallicity gradients in their discs although the gradients can be seen in the case of weak feedback. Our simulations would correspond to the case of weak feedback, therefore we could expect that the weak metallicity relations in this study would be due to the violent perturbation by the massive clumps. However, metallicity of the disc stars would become lower than our simulations if the other feedback processes are implemented.

Our simulations are, in addition, not cosmological; our models are lacking continuous gas accretion which is expected to feed thin discs. The thin-disc formation could shorten the scale heights of the thick discs and might influence the velocity dispersions. In the cosmological context, smooth and cold gas streams are thought to penetrate a halo and keep a galaxy gas-rich until the streams are turned off in the high-redshift Universe (e.g. Dekel & Birnboim 2006; Dekel et al. 2009). As noted in §3.1.1, gas fraction in the clumps may affect some properties of the clump-origin bulges such as density profile and mass. In isolated models like our simulations, properties of giant clumps would be more or less controlled by the initial settings. For example, spin parameter is responsible for mass function of clumps: Small and large spin parameters of the initial conditions lead to high and low surface gas density of the discs. The wavelength at which dynamical instability first

appears becomes longer in a disc with a higher surface density, which allows to form more massive clumps preferentially (Toomre 1964; Binney & Tremaine 2008). This inference can be seen in Fig.12: In B01- $\lambda 010$ and K11- $\lambda 010$, more clumps of $\gtrsim 10^8 M_\odot$ formed than in the runs of B01- $\lambda 004$ and K11- $\lambda 004$. As we showed in §3, however, the kinematic and chemical properties of the thick discs in our simulations are qualitatively consistent between the runs and do not seem to depend very much on the initial conditions.

4.2 The thick disc formation in clumpy galaxies

Here we inspect how realistic the scenario of thick-disc formation in clumpy galaxies is. As Bournaud et al. (2009) showed, the thick-disc formation in clumpy galaxies has the advantages that constant thickness and old age of thick discs can be well reproduced in agreement with observations. These were confirmed in our simulations. In the scenarios of thin disc heating and radial migration, thick discs seem to form with scale heights increasing with galactocentric radius, i.e. flaring thick discs (Kazantzidis et al. 2008; Minchev et al. 2012), although radial migration seems able to explain the relation between $\overline{v_\theta}$ and metallicity (Curir et al. 2012). In our simulations, although the scale radii of the discs were contingent to the initial rotation of gas, the scale heights of $h_T \simeq 1$ kpc seem to be consistent with observed thick discs and almost independent of the initial conditions. Significant asymmetric drift, $d\overline{v_\theta}/dz$, was also confirmed in the runs of B01- $\lambda 004$ and K11- $\lambda 004$. Radial profiles of velocity dispersions except σ_R were also nearly exponential. The pioneering work of Lewis & Freeman (1989) has observed exponential decrease of σ_R and σ_θ for old disc stars with scale lengths similar to that of surface density, whereas Casetti-Dinescu et al. (2011) observed the only significant radial gradient of σ_z in the MW thick-disc stars. Moreover, we found that vertical profiles of velocity dispersions are almost isothermal in our simulations. In observations of the MW thick disc, Moni Bidin et al. (2012) have observed velocity dispersion profiles weakly increasing with height above the plane (although see Sanders 2012); however, some observations indicated steep vertical gradients of σ_R (Casetti-Dinescu et al. 2011) and σ_z (Kordopatis et al. 2011). Distributions of orbital eccentricities in the entire thick discs in our simulations showed excellent agreement with observations of the MW thick disc. However, vertical dependence of the eccentricities cannot be reproduced. Thus, we can see that the comparisons of dynamical properties between our simulations and the observations do not indicate evident discrepancies, except the vertical variation of orbital eccentricities observed in the MW (Dierickx et al. 2010).

We found that metallicity gradients are quite weak in our simulations. In observations of the MW, thick-disc stars do not seem to have steep metallicity gradients in radial or vertical directions (e.g. Allende Prieto et al. 2006; Bensby et al. 2011; Ruchti et al. 2011; Kordopatis et al. 2011; Carrell et al. 2012). However, our simulations did not show metallicity relations with orbital eccentricities and rotation velocities, which have recently been observed in the MW thick disc (Lee et al. 2011; Kordopatis et al. 2011, 2013). We consider that this lack of chemo-dynamical relations is the most striking discrepancy between our sim-

ulations and the observations. We infer that disc stars are stirred by violent perturbation of giant clumps and such chemo-dynamical relations would be washed out in the clumpy phase. In the observations of Lee et al. (2011), their samples of thin- and thick-disc stars showed distinct chemo-dynamical relations, this is thought to reflect distinct formation processes of these discs. Thus, the chemical relations are expected to be susceptible to formation scenarios of discs, and the inconsistency between our simulations and the observations of the MW implies that the thick-disc formation scenario in clumpy galaxies may not be suitable for the MW.

Tadaki et al. (2014) have observed that 41 per cent of H α emitters of stellar masses from 10^9 to $10^{11.5} M_{\odot}$ have clumpy morphologies at redshifts of 2.2 and 2.5, and the fraction of clumpy galaxies becomes the largest at the mass of $10^{10.5} M_{\odot}$. However, van Dokkum et al. (2013) observationally argued that MW progenitors would have stellar masses of $10^{9.5}$ – $10^{10} M_{\odot}$ in this redshift range (see their fig. 1). From these observations, typical clumpy galaxies may be too massive to evolve into the MW-size galaxies. If it is the case, the thick-disc formation in a clumpy disc would not be suitable for the MW and smaller galaxies.

It should be noted, however, that thick discs in external galaxies show a wide variety of kinematic properties, which is discussed to correlate with Hubble types and/or galaxy masses (e.g. Yoachim & Dalcanton 2006, 2008; Comerón et al. 2011). Presumably, this may mean that the formation process of thick discs is not a single scenario and the diverse kinematics of the thick discs could be the consequence of the variety of formation history. Observational studies of chemo-dynamical properties of thick-disc stars in external galaxies are, unfortunately, far from sufficient. First, orbital eccentricity of each thick-disc star is not observable in these galaxies since three-dimensional position and velocity of a star are not accessible even if we could resolve its stellar image. However, it may be possible to observe the relation between metallicity and rotation velocity. Yoachim & Dalcanton (2008) have observed some edge-on galaxies and obtained rotation curves at different height above disc planes. They found that relatively massive galaxies in their sample do not indicate significant vertical gradient of rotation velocities. On the other hand, their less massive galaxies show a wide range of behaviour such as counter-rotation between thin and thick discs, but they tend to indicate asymmetric drift more clearly than the massive galaxies. If altitudinal dependence of metallicity is observed in these galaxies, one can discuss whether they have a chemo-dynamical relation like the MW thick disc and whether it is a universal relation or not.

The authenticity of the clear distinction between the thin and thick discs is still under discussion, and the Galactic thick disc may be a superposition of relatively old components which are continuously connected to the thin disc (e.g. Dove & Thronson 1993; Bovy et al. 2012a,b,c; Stinson et al. 2013). Bovy et al. (2012c) discussed that each component consisting of the Galactic disc is a simple structure with a single exponential density profile and isothermal kinematics. Recent observations by Haywood et al. (2013), however, indicated that the Galactic thick- and thin-disc stars have obviously distinguishable age- $[\alpha/\text{Fe}]$ and $-\text{[Fe/H]}$ relations although the durations of their star formation somewhat overlap. Their result would prefer distinct formation pro-

cesses between the thin and thick discs. They discussed the formation epoch of the thick disc to be the first 4–5 Gyr of the Galaxy formation with starburst; this period corresponds to redshift of $z = 2$ –3. Thus, further investigation is needed to obtain more detailed and accurate information for the Galactic thick disc. In addition, observations for external galaxies are also essential to compare with the MW and inspect the universality and individuality of thick discs.

5 CONCLUSIONS

In this study, we found that properties of thick discs are almost consistent among our runs with different initial conditions. Our simulations indicated that kinematic properties such as density and velocity profiles and distributions of orbital eccentricities are in acceptable agreement with Galactic and external galactic observations. However, altitudinal dependence of the eccentricities and metallicity relations with rotation velocities and eccentricities are not confirmed in our simulations, which are discrepant from recent observations of the Galactic thick disc. Therefore, we infer that the thick-disc formation scenario by clumpy discs would not be suitable at least for the MW.

ACKNOWLEDGMENTS

We would like to thank the referee for a careful reading of the manuscript and useful comments. We are grateful to Daisuke Kawata, Junichi Baba, Kohei Hattori, Shunsuke Hozumi, Ken-ichi Tadaki, Daniel Ceverino and Avishai Dekel for their helpful discussion. The numerical simulations reported here were carried out on Cray XT-4 kindly made available by CfCA (Center for Computational Astrophysics) at the National Astronomical Observatory of Japan.

REFERENCES

- Abadi M. G., Navarro J. F., Steinmetz M., Eke V. R., 2003, *ApJ*, 597, 21
- Agertz O., Kravtsov A. V., Leitner S. N., Gnedin N. Y., 2013, *ApJ*, 770, 25
- Agertz O., Teyssier R., Moore B., 2009, *MNRAS*, 397, L64
- Allende Prieto C., Beers T. C., Wilhelm R., Newberg H. J., Rockosi C. M., Yanny B., Lee Y. S., 2006, *ApJ*, 636, 804
- Bensby T., Alves-Brito A., Oey M. S., Yong D., Meléndez J., 2011, *ApJL*, 735, L46+
- Binney J., Merrifield M., 1998, *Galactic Astronomy*. Princeton Univ. Press, Princeton
- Binney J., Tremaine S., 2008, *Galactic Dynamics Second Edition*. Princeton Univ. Press, Princeton
- Bouché N., et al., 2007, *ApJ*, 671, 303
- Bournaud F., Elmegreen B. G., 2009, *ApJ*, 694, L158
- Bournaud F., Elmegreen B. G., Elmegreen D. M., 2007, *ApJ*, 670, 237
- Bournaud F., Elmegreen B. G., Martig M., 2009, *ApJL*, 707, L1
- Bournaud F., et al., 2014, *ApJ*, 780, 57
- Bovy J., Rix H.-W., 2013, preprint (astro-ph/1309.0809)
- Bovy J., Rix H.-W., Hogg D. W., 2012a, *ApJ*, 751, 131

- Bovy J., Rix H.-W., Hogg D. W., Beers T. C., Lee Y. S., Zhang L., 2012b, *ApJ*, 755, 115
- Bovy J., Rix H.-W., Liu C., Hogg D. W., Beers T. C., Lee Y. S., 2012c, *ApJ*, 753, 148
- Brook C. B., et al., 2012, *MNRAS*, 426, 690
- Brook C. B., Gibson B. K., Martel H., Kawata D., 2005, *ApJ*, 630, 298
- Brook C. B., Kawata D., Gibson B. K., Freeman K. C., 2004, *ApJ*, 612, 894
- Buitrago F., Conselice C. J., Epinat B., Bedregal A. G., Grutzbauch R., 2013, preprint (astro-ph/1305.0268)
- Bullock J. S., Dekel A., Kolatt T. S., Kravtsov A. V., Klypin A. A., Porciani C., Primack J. R., 2001, *ApJ*, 555, 240
- Burstein D., 1979, *ApJ*, 234, 829
- Carollo D., Beers T. C., Chiba M., Norris J. E., Freeman K. C., Lee Y. S., Ivezić Ž., Rockosi C. M., Yanny B., 2010, *ApJ*, 712, 692
- Carrell K., Chen Y., Zhao G., 2012, *AJ*, 144, 185
- Casetti-Dinescu D. I., Girard T. M., Korchagin V. I., van Altena W. F., 2011, *ApJ*, 728, 7
- Ceverino D., Dekel A., Bournaud F., 2010, *MNRAS*, 404, 2151
- Ceverino D., Dekel A., Mandelker N., Bournaud F., Burkert A., Genzel R., Primack J., 2012, *MNRAS*, 420, 3490
- Cha S.-H., Whitworth A. P., 2003, *MNRAS*, 340, 91
- Chen Y. Q., Zhao G., Carrell K., Zhao J. K., 2011, *AJ*, 142, 184
- Cheng J. Y., et al., 2012a, *ApJ*, 752, 51
- Cheng J. Y., et al., 2012b, *ApJ*, 746, 149
- Chiba M., Beers T. C., 2000, *AJ*, 119, 2843
- Coşkunoglu B., Ak S., Bilir S., Karaali S., Önal Ö., Yaz E., Gilmore G., Seabroke G. M., 2012, *MNRAS*, 419, 2844
- Comerón S., et al., 2011, *ApJ*, 741, 28
- Curir A., Lattanzi M. G., Spagna A., Matteucci F., Murante G., Re Fiorentin P., Spitoni E., 2012, *A&A*, 545, A133
- Dalcanton J. J., Bernstein R. A., 2002, *AJ*, 124, 1328
- Dalla Vecchia C., Schaye J., 2012, *MNRAS*, 426, 140
- Dekel A., Birnboim Y., 2006, *MNRAS*, 368, 2
- Dekel A., et al., 2009, *Nature*, 457, 451
- Dekel A., Krumholz M. R., 2013, preprint (astro-ph/1302.4457)
- Dekel A., Sari R., Ceverino D., 2009, *ApJ*, 703, 785
- Del Popolo A., Hiotelis N., 2014, *JCAP*, 1, 47
- Dierickx M., Klement R., Rix H.-W., Liu C., 2010, *ApJ*, 725, L186
- Dove J. B., Thronson Jr. H. A., 1993, *ApJ*, 411, 632
- Drory N., Fisher D. B., 2007, *ApJ*, 664, 640
- Dutton A. A., et al., 2011, *MNRAS*, 410, 1660
- Elmegreen B. G., Bournaud F., Elmegreen D. M., 2008a, *ApJ*, 688, 67
- Elmegreen B. G., Bournaud F., Elmegreen D. M., 2008b, *ApJ*, 684, 829
- Elmegreen B. G., Elmegreen D. M., 2005, *ApJ*, 627, 632
- Elmegreen B. G., Elmegreen D. M., 2006, *ApJ*, 650, 644
- Elmegreen B. G., Elmegreen D. M., Vollbach D. R., Foster E. R., Ferguson T. E., 2005, *ApJ*, 634, 101
- Elmegreen B. G., Struck C., 2013, *ApJ*, 775, L35
- Elmegreen D. M., Elmegreen B. G., Hirst A. C., 2004, *ApJL*, 604, L21
- Elmegreen D. M., Elmegreen B. G., Marcus M. T., Shahinyan K., Yau A., Petersen M., 2009, *ApJ*, 701, 306
- Fathi K., 2010, *ApJ*, 722, L120
- Fathi K., Allen M., Boch T., Hatziminaoglou E., Peletier R. F., 2010, *MNRAS*, 406, 1595
- Fisher D. B., Drory N., 2008, *AJ*, 136, 773
- Forbes J. C., Krumholz M. R., Burkert A., Dekel A., 2013, ArXiv e-prints
- Förster Schreiber N. M., et al., 2006, *ApJ*, 645, 1062
- Förster Schreiber N. M., et al., 2011, *ApJ*, 739, 45
- Fuhrmann K., 2008, *MNRAS*, 384, 173
- Genel S., et al., 2012, *ApJ*, 745, 11
- Genzel R., et al., 2006, *Nature*, 442, 786
- Genzel R., et al., 2011, *ApJ*, 733, 101
- Gibson B. K., Pilkington K., Brook C. B., Stinson G. S., Bailin J., 2013, *A&A*, 554, A47
- Gilmore G., Reid N., 1983, *MNRAS*, 202, 1025
- Gingold R. A., Monaghan J. J., 1983, *MNRAS*, 204, 715
- Guo Y., Gialvalisco M., Ferguson H. C., Cassata P., Koekoemoer A. M., 2012, *ApJ*, 757, 120
- Hayden M. R., et al., 2013, ArXiv e-prints
- Haywood M., Di Matteo P., Lehnert M., Katz D., Gomez A., 2013, preprint (astro-ph/1305.4663)
- Hernquist L., 1990, *ApJ*, 356, 359
- Hopkins P. F., Quataert E., Murray N., 2012, *MNRAS*, 421, 3522
- Immeli A., Samland M., Gerhard O., Westera P., 2004, *A&A*, 413, 547
- Inoue S., 2013, *A&A*, 550, A11
- Inoue S., Saitoh T. R., 2011, *MNRAS*, 418, 2527
- Inoue S., Saitoh T. R., 2012, *MNRAS*, 422, 1902
- Ishiyama T., Rieder S., Makino J., Portegies Zwart S., Groen D., Nitadori K., de Laat C., McMillan S., Hiraki K., Harfst S., 2013, *ApJ*, 767, 146
- Jensen E. B., Thuan T. X., 1982, *ApJS*, 50, 421
- Jurić M., et al., 2008, *ApJ*, 673, 864
- Katz D., Soubiran C., Cayrel R., Barbuy B., Friel E., Binaimé O., Perrin M.-N., 2011, *A&A*, 525, A90
- Kaufmann T., Mayer L., Wadsley J., Stadel J., Moore B., 2006, *MNRAS*, 370, 1612
- Kaufmann T., Mayer L., Wadsley J., Stadel J., Moore B., 2007, *MNRAS*, 375, 53
- Kazantzidis S., Bullock J. S., Zentner A. R., Kravtsov A. V., Moustakas L. A., 2008, *ApJ*, 688, 254
- Kent S. M., 1985, *ApJS*, 59, 115
- Kimm T., Devriendt J., Slyz A., Pichon C., Kassin S. A., Dubois Y., 2011, preprint (astro-ph/1106.0538)
- Kordopatis G., et al., 2011, *A&A*, 535, A107
- Kordopatis G., et al., 2013, *MNRAS*, 436, 3231
- Kormendy J., Kennicutt Jr. R. C., 2004, *ARA&A*, 42, 603
- Krumholz M. R., Dekel A., 2010, *MNRAS*, 406, 112
- Kuijken K., Gilmore G., 1989, *MNRAS*, 239, 571
- Lee Y. S., et al., 2011, *ApJ*, 738, 187
- Lewis J. R., Freeman K. C., 1989, *AJ*, 97, 139
- Makino J., 1991, *ApJ*, 369, 200
- Makino J., 2004, *PASJ*, 56, 521
- Mandelker N., Dekel A., Ceverino D., Tweed D., Moody C. E., Primack J., 2013, preprint (astro-ph/1311.0013)
- Matthews L. D., 2000, *AJ*, 120, 1764
- McMillan S. L. W., 1986, in Hut P., McMillan S. L. W., eds, *The Use of Supercomputers in Stellar Dynamics* Vol. 267

of Lecture Notes in Physics, Berlin Springer Verlag, The Vectorization of Small-N Integrators. p. 156

Minchev I., Famaey B., Quillen A. C., Dehnen W., Martig M., Siebert A., 2012, *A&A*, 548, A127

Miyamoto M., Nagai R., 1975, *PASJ*, 27, 533

Monaghan J. J., 1992, *ARA&A*, 30, 543

Moni Bidin C., Carraro G., Méndez R. A., 2012, *ApJ*, 747, 101

Navarro J. F., Frenk C. S., White S. D. M., 1997, *ApJ*, 490, 493

Newman S. F., et al., 2012, *ApJ*, 752, 111

Noguchi M., 1996, *ApJ*, 469, 605

Noguchi M., 1998, *Nat*, 392, 253

Noguchi M., 1999, *ApJ*, 514, 77

Nordström B., Mayor M., Andersen J., Holmberg J., Pont F., Jørgensen B. R., Olsen E. H., Udry S., Mowlavi N., 2004, *A&A*, 418, 989

Perez J., Valenzuela O., Tissera P. B., Michel-Dansac L., 2013, *MNRAS*, 436, 259

Quinn P. J., Hernquist L., Fullagar D. P., 1993, *ApJ*, 403, 74

Ruchti G. R., et al., 2011, *ApJ*, 737, 9

Saitoh T. R., Daisaka H., Kokubo E., Makino J., Okamoto T., Tomisaka K., Wada K., Yoshida N., 2008, *PASJ*, 60, 667

Saitoh T. R., Daisaka H., Kokubo E., Makino J., Okamoto T., Tomisaka K., Wada K., Yoshida N., 2009, *PASJ*, 61, 481

Saitoh T. R., Makino J., 2009, *ApJL*, 697, L99

Saitoh T. R., Makino J., 2010, *PASJ*, 62, 301

Saitoh T. R., Makino J., 2012, *New Astron.*, 17, 76

Saitoh T. R., Makino J., 2013, *ApJ*, 768, 44

Sales L. V., et al., 2009, *MNRAS*, 400, L61

Salpeter E. E., 1955, *ApJ*, 121, 161

Sanders J., 2012, *MNRAS*, 425, 2228

Schmidt M., 1959, *ApJ*, 129, 243

Schönrich R., Binney J., 2009a, *MNRAS*, 396, 203

Schönrich R., Binney J., 2009b, *MNRAS*, 399, 1145

Shaw M. A., Gilmore G., 1990, *MNRAS*, 242, 59

Spagna A., Lattanzi M. G., Re Fiorentin P., Smart R. L., 2010, *A&A*, 510, L4

Springel V., 2010, *ARA&A*, 48, 391

Stinson G., Seth A., Katz N., Wadsley J., Governato F., Quinn T., 2006, *MNRAS*, 373, 1074

Stinson G. S., Brook C., Prochaska J. X., Hennawi J., Shen S., Wadsley J., Pontzen A., Couchman H. M. P., Quinn T., Macciò A. V., Gibson B. K., 2012, *MNRAS*, 425, 1270

Stinson G. S., et al., 2013, *MNRAS*, 436, 625

Swinbank M., Smail I., Sobral D., Theuns T., Best P., Geach J., 2012, preprint (astro-ph/1209.1396)

Tadaki K.-i., Kodama T., Tanaka I., Hayashi M., Koyama Y., Shimakawa R., 2014, *ApJ*, 780, 77

Tanikawa A., Yoshikawa K., Nitadori K., Okamoto T., 2013, *New Astron.*, 19, 74

Teyssier R., Pontzen A., Dubois Y., Read J. I., 2013, *MNRAS*, 429, 3068

Toomre A., 1964, *ApJ*, 139, 1217

van den Bergh S., Abraham R. G., Ellis R. S., Tanvir N. R., Santiago B. X., Glazebrook K. G., 1996, *AJ*, 112, 359

van der Kruit P. C., Freeman K. C., 2011, *ARA&A*, 49, 301

van der Kruit P. C., Searle L., 1981, *A&A*, 95, 105

van Dokkum P. G., et al., 2013, *ApJ*, 771, L35

Wada K., Papadopoulos P. P., Spaans M., 2009, *ApJ*, 702, 63

Wuyts S., et al., 2012, *ApJ*, 753, 114

Yoachim P., Dalcanton J. J., 2006, *AJ*, 131, 226

Yoachim P., Dalcanton J. J., 2008, *ApJ*, 682, 1004

Yoshii Y., 1982, *PASJ*, 34, 365

APPENDIX A: ROBUSTNESS OF THE ECCENTRICITY DETERMINATION

Here we discuss how robust the eccentricity distributions presented in Fig. 9 are with respect to the modeling of galactic discs. The computation of stellar eccentricities have to model the mass distribution of the galaxies and might be significantly affected by our choice of the models. Especially, the disc model — which is the only non-spherical component in the galaxy model — may have a large impact on the eccentricity determinations.

In §3.2.3, our eccentricity determinations assumed the Miyamoto-Nagai discs (Miyamoto & Nagai 1975) for the sake of consistency with the analyses of Lee et al. (2011), and the structural parameters were chosen to fit with the circular velocity curves of the simulated galaxies. As shown in §3.1.2, however, the density profiles of the stellar discs are fitted with the double-exponential models of equation (2). In this appendix, we perform the same analyses for computing orbital eccentricities using the exponential models instead of the Miyamoto-Nagai discs. The radial and vertical forces, K_R and K_z , caused by the exponential disc are given as

$$K_{R,i}(R, z) = -4\pi G\alpha_i\rho_{0,i} \int_0^\infty kdkJ_1(kR)(\alpha_i^2 + k^2)^{-\frac{3}{2}} \times \frac{\beta_i e^{-k|z|} - ke^{-\beta_i|z|}}{\beta_i^2 - k^2} \quad (\text{A1})$$

and

$$K_{z,i}(R, z) = -4\pi G\alpha_i\rho_{0,i} \int_0^\infty dkJ_0(kR)(\alpha_i^2 + k^2)^{-\frac{3}{2}} \times k\beta_i \text{sign}(z) \frac{\beta_i e^{-k|z|} - ke^{-\beta_i|z|}}{\beta_i^2 - k^2}, \quad (\text{A2})$$

where $J_{0,1}$ are Bessel functions of the first kind, $\alpha_i \equiv R_i^{-1}$ and $\beta_i \equiv h_i^{-1}$ (Kuijken & Gilmore 1989). The density models for the bulges and halos are the same as in §3.1. Although density distribution of gas seems different from the stellar discs in our simulations, we assume that the gas follows the thin-disc model.

Fig. A1 shows the eccentricity distribution computed using the exponential disc models. In the top panel, we compare the eccentricities with the results in Fig. 9. The eccentricity distributions are almost the same in the runs of B01- λ 004 and K11- λ 004. Although the distributions become to have a little higher averages and large dispersions in B01- λ 010 and K11- λ 010, our results do not change qualitatively. The bottom panel shows dependence of the distributions on distance from the planes. Systematic difference from the case using the Miyamoto-Nagai discs cannot be seen, and the distributions are still independent from the distance from the galactic planes. Hence, we can see that

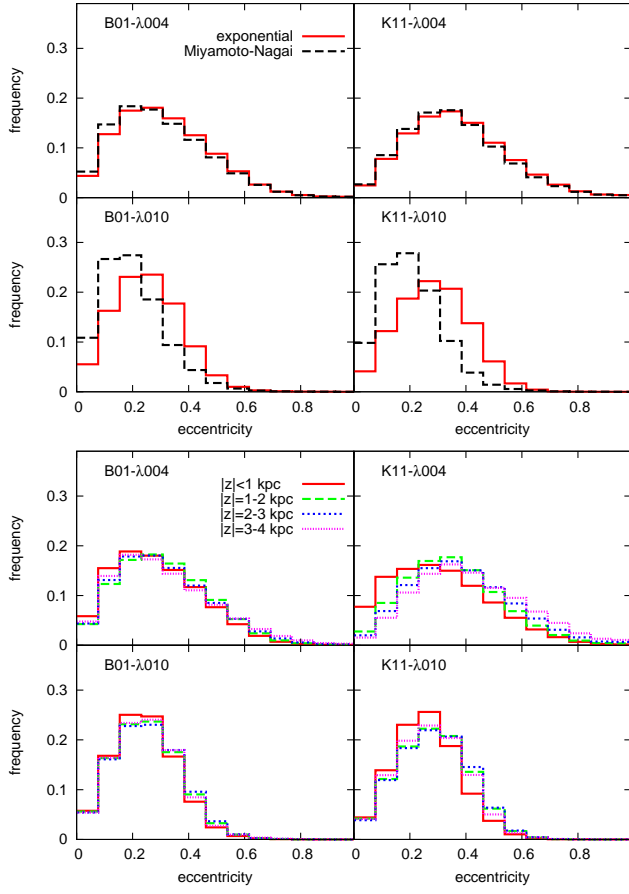


Figure A1. The same as Fig. 9 but using the double-exponential models for the thick and thin discs. In the top panel, the black dashed histogram indicates the result of Fig. 9 where the Miyamoto–Nagai disc model is used.

the eccentricity determinations in this study do not depend on the details of the galaxy models.